Hybrid Quantum and Classical Simulations of the Formate Dehydrogenase Catalyzed Hydride Transfer Reaction on an Accurate Semiempirical Potential Energy Surface

Alexandra Vardi-Kilshtain,[†] Dan Thomas Major,*,[†] Amnon Kohen,[‡] Hamutal Engel,[†] and Dvir Doron[†]

[†]Department of Chemistry and the Lise Meitner-Minerva Center of Computational Quantum Chemistry, Bar-Ilan University, Ramat-Gan 52900, Israel

[‡]Department of Chemistry, University of Iowa, Iowa City, Iowa 52242, United States

S Supporting Information

ABSTRACT: Formate dehydrogenase (FDH) catalyzes the oxidation of formic acid to carbon dioxide using nicotinamide adenine dinucleotide (NAD$^+$) as a cofactor. In the current work we present extensive benchmark calculations for several model reactions in the gas phase that are relevant to the FDH catalyzed hydride transfer. To this end we employ G4MP2 and CBS-QB3 ab initio calculations as well as density functional theory methods. Using these results we develop a specific reaction parameter (SRP) Hamiltonian based on the semiempirical AM1 method. The SRP semiempirical Hamiltonian is subsequently used in hybrid quantum mechanics/molecular mechanics simulations of the FDH catalyzed reaction in *Pseudomonas* sp. 101 (*Pse*FDH). The classical potential of mean force (PMF) is computed as a function of structural progress coordinates during the course of the hydride transfer reaction: The antisymmetric reactive stretch, the donor−acceptor distance, and an orbital rehybridization coordinate. The quantum PMF is computed using a centroid Feynman path-integral (PI) approach. Subsequently, kinetic isotope effects are computed using a mass-perturbation based PI method. Finally, the antisymmetric stretch vibrational frequency is computed for an azide ion in FDH and in aqueous solution.

1. INTRODUCTION

Nicotinamide adenine dinucleotide (NAD$^+$)-dependent formate dehydrogenase (EC 1.2.1.2; FDH) oxidizes the formate ion to carbon dioxide in conjunction with the reduction of NAD$^+$ to NADH. FDH is a ubiquitous enzyme belonging to a family of D-isomer-specific 2-hydroxyacid dehydrogenases[1] and plays a key role in the energy supply of microorganisms and in the stress response in plants.[2]

In addition to being an important NAD$^+$-dependent dehydrogenase, FDH has several practical applications. FDH is often used as a catalyst for NADH regeneration in the synthesis of chiral compounds with NAD$^+$-dependent dehydrogenases.[3,4] Indeed, due to the high activity of FDH in a wide pH window, the irreversibility of the enzymatic reaction, and its high solubility, FDH is employed as a biocatalyst in many chemical processes. An example of the use of the enzyme in cofactor regeneration in a large scale industrial process is the production of a biosynthetic amino acid, *tert*-L-leucine, which is a component of some HIV protease and matrix metalloprotease inhibitors.[5]

Kinetic and X-ray diffraction studies have established that FDH binds NAD$^+$ prior to formate binding. Subsequently, a direct transfer of a hydride ion from the formate anion to the *pro*-R C4 position of the nicotinamide ring of NAD$^+$ occurs in the ternary complex, forming carbon dioxide and NADH (Scheme 1).[6,7] The hydride transfer step is partly rate limiting in the catalytic mechanism of FDH, thus the Northrop method has been used to expose the intrinsic KIEs.[8] FDH has been employed extensively as a model system in the study of hydride-ion transfers in NAD$^+$-dependent dehydrogenases.[9−11]

Scheme 1. Hydride Transfer Reaction Catalyzed by FDH[a]
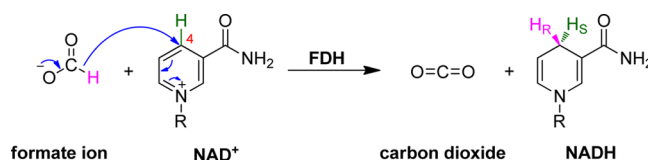
^{a}R: adenine dinucleotide.

FDH crystal structures have been solved for 3 species: the methylotrophic bacterium *Pseudomonas* sp. 101 (*Pse*FDH),[12] the methylotrophic bacterium *Moraxella* C-1 (*Mor*FDH),[13] and the Yeast *Candida boidinii* (*Cbo*FDH).[14] FDH is a homodimer consisting of two 42 kDa subunits, each composed of two domains: the coenzyme binding domain and the catalytic domain. The enzyme active site is positioned in a deep cleft separating the two domains.[12,14] FDH can exist in different well-defined states as is typical for enzymes, the principal ones being the so-called open and closed conformations. Intertransition between the open and closed conformations is essential for the formation and sequestering of the enzyme active site as well as for catalysis. The cofactor is an important player in the transition between the open and closed states of the enzyme, as it acts as a bridge between the two domains.[12,13] Analysis of the crystallographic structures suggests that the cofactor and substrate are involved in multiple interactions in the active site.[15,16]

Detailed theoretical and kinetic studies of FDH have been performed in an attempt to delineate the transition state (TS) structure as well as the catalytic effect of the enzyme.[17−27] Several theoretical studies suggested that puckering of the pyridine ring can reduce the activation barrier.[18−23] However, the small measured secondary ^{15}N kinetic isotope effects (KIE) at the N1 position of 3-acetylpyridine adenine dinucleotide on the reaction catalyzed by FDH[24] and gas-phase *ab initio* calculations[25,26] suggest that N1 does not experience a significant decrease in bond order during the chemical step.[24] Additional KIEs have been measured for yeast FDH by Blanchard and Cleland, such as ^{13}C at the C4 position and primary deuterium KIEs, yielding values of 1.043 and 2.8, respectively.[27] Interestingly, this measured deuterium isotope effect is relatively low compared with those reported for other dehydrogenases. Blanchard and Cleland suggested that this relatively low value reflects a late TS. This conclusion was also supported by the relative large [13]C4 effect and the behavior of azide as a TS analogue.[27] Blanchard and Cleland also measured [2]H-KIE values of 4.4 for thio-NAD, 6.9 for acetylpyridine-NAD, and 3.8 for pyridinecarboxaldehyde-NAD, which would represent earlier TSs.[27]

In FDH, quantum mechanical tunneling has been indicated based on KIE studies.[9,28,8] Recently, Kohen and co-workers studied the environmental dynamics of *Cbo*FDH in complex with azide and nicotinamide (NAD^{+}), using infrared photon-echo spectroscopy. These studies revealed structural fluctuations on the ps to fs time scale, which could be relevant to catalysis.[9] Additionally, the intrinsic KIEs were found to be temperature independent, with isotopic ratios of Arrhenius pre-exponential factors above the semiclassical limits, indicating deviation from semiclassical, nontunneling, models.[8] Together, the spectroscopic and kinetic measurements suggest that near the so-coined "tunneling-ready conformation", the FDH complex may be optimized for hydrogen tunneling.

Theoretical studies of the catalytic mechanism of *Pse*FDH were carried out recently by Moliner, Tuñón, and co-workers using quantum mechanics/molecular (QM/MM) mechanics techniques.[10,29] Their results showed a 12.4 kcal/mol free energy barrier for the reaction in the enzyme in comparison to 21.3 kcal/mol in solution. They concluded that the catalytic effect is due to substrate preorganization and TS stabilization with respect to aqueous solution, thus diminishing the activation barrier. In this work, a standard semiempirical AM1 Hamiltonian[30] was employed, and *ab initio* single-point calculations were used to correct for the inherent deficiencies of AM1.
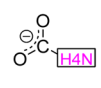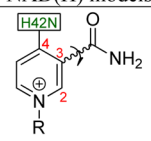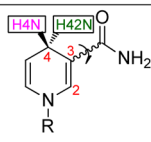
In this paper, we initially present gas-phase model calculations for the hydride transfer reaction between the formate ion and NAD^{+}, using high-level *ab initio* and density functional theory (DFT) methods. Based on these high-level calculations, we derive a semiempirical specific reaction parameter (SRP) set for the FDH catalyzed hydride transfer reaction.[31−33] This efficient and accurate potential energy surface (PES) is employed in hybrid quantum mechanics/molecular mechanics (QM/MM)[34] free energy simulations with the full solvated enzyme. Nuclear quantum effects (NQE) are described using a coupled free-energy mass-perturbation and umbrella sampling simulation technique based on Feynman centroid path integral calculations (PI-FEP/UM).[35] Thus, both the electronic structure of the reacting system and the nuclear dynamics are treated quantum mechanically. This method has been successfully employed in a series of studies of chemical reactions in solution and in enzymes.[32,33,35−38] Finally, the antisymmetric stretch frequency is computed for an azide ion in FDH and in aqueous solution using a thermal density matrix diagonalization approach.[38]

2. METHODOLOGY

2.1. Gas-Phase QM Calculations. *Model Reactions.* The molecules presented in Chart 1 are chemical analogues of the

Chart 1. Main Models Used in Gas-Phase Calculations in This Study[a]

[a]The labels of the hydrogen atoms involved in the calculation of the primary and secondary kinetic isotope effects (H4N and H42N, respectively) are framed and colored in accordance with Scheme 1.

reacting ligands and their corresponding products in the FDH enzymatic reaction. The geometries were fully optimized in the gas phase using the Gaussian09 program[39] with two different density functionals, the hybrid GGA functional, B3LYP,[40−42] and the hybrid meta-GGA functional, M06,[43] in conjunction with the 6-31+G(d,p) basis set. The same molecules were minimized with the semiempirical Hamiltonian Austin Model 1 (AM1).[30] We also carried out high level calculations with the Complete Basis Set method CBS-QB3[44,45] as well as the Gaussian theory method G4MP2.[46,47] The latter method provided most of the target values for reparametrization of the AM1 Hamiltonian (*vide infra*). Several additional DFT methods were tested, and M06 yielded the best agreement with the high-level *ab initio* data (results not shown).

Two conformers of the nicotinamide derivative representing the NAD(H) cofactor were considered, differing in the orientation of the carboxamide with respect to the (dihydro)-pyridine ring: the *cisoid* conformer, in which the carbonyl group and the C2=C3 bond are quasi-synperiplanar, and the *transoid* conformer, where these two are quasi-antiperiplanar. As the two types of conformers were taken into account for both the reduced and oxidized nicotinamide species (Me-H$_2$nic and Me-Hnic[+], respectively), two thermodynamic pathways were computed for each model reaction.

In both model reactions, the changes in electronic energy (ΔE_{el}), enthalpy (ΔH), and Gibbs free energy (ΔG) at 298 K were computed for each pathway with the above-mentioned methods, according to the general equation

$$\Delta X_r = X[\text{CO}_2] + X[\textit{cis/trans}\text{-Me-H}_2\text{nic}] - X[\text{HCOO}^-]$$

$$- X[\textit{cis/trans}\text{-Me-Hnic}^+] \tag{1}$$

where X is a general notation for E_{el}, H, or G.

Standard harmonic statistical mechanics expressions were employed in the calculation of ΔH and ΔG.[48]

Modeling the Reactant, Transition, and Product State Complexes. The optimized model structure for the TS complex in aqueous solution was found using the Synchronous Transit-Guided Quasi-Newton (STQN) method[49] implemented in the Gaussian09 program,[39] with B3LYP/6-31+G(d,p) and M06/6-31+G(d,p) with the integral equation formalism polarizable continuum model (IEF-PCM),[50] excluding nonelectrostatic contributions. The *transoid* conformer of the Me-Hnic[+] subunit was chosen, because it was found to be the most prevalent conformer identified in X-ray crystal structures of most enzyme active sites,[51,52] in particular *Pse*FDH.[12] The saddle point was identified by a single imaginary vibrational frequency corresponding to the normal mode of the hydride transfer between the donor (C in the formic acid) and acceptor (C4N in the nicotinamide subunit) carbons.

The reactant state (RS) and product state (PS) complexes, $[\text{HCOO}^- \bullet trans\text{-Me-Hnic}^+]$ and $[\text{CO}_2 \bullet trans\text{-Me-H}_2\text{nic}]$, respectively, were obtained by intrinsic reaction coordinate (IRC) calculations in the direction of reactants and products in aqueous solution with the IEF-PCM approach.[50] The steepest descent path in mass-scaled coordinates was followed in steps of 0.1 Bohr in each direction of the reaction path down to the reactant and product complex wells, until the default convergence criteria were reached in each IRC direction.

Development of Semiempirical Specific Reaction Parameters. In the current SRP approach,[31] the semiempirical parameters are optimized for the hydride transfer reaction in FDH. The approach closely follows the strategy adopted for DHFR, which has been described previously, and will therefore only be presented briefly here.[53] AM1-SRP parameters are developed to reproduce electronic and thermodynamic properties obtained from high-level QM calculations on model molecules in the gas phase and in solution. The molecular models employed in the parametrization of AM1 included both individual gas-phase molecules (Chart 1) and the bimolecular complexes of the RS, TS, and PS in aqueous solution (*vide supra*). In total, 12 individual molecules were employed in the parametrization process (Chart 1, *cis*- and *trans*-neutral nicotinamides are not shown; see also Table 2) and three bimolecular complexes. The reference method for the AM1 parametrization was the composite Gaussian method G4MP2,[46,47] whereas target quantities associated with models of the reactant, transition, and product state bimolecular complexes were calculated using the M06 hybrid functional[43] with the 6-31+G(d,p) basis set. The observables used as target values were enthalpies of formation, reaction energies, geometries, dipole moments, Mulliken charges, and vibrational frequencies. The SRP parameters are obtained by a nonlinear optimization, starting with the original AM1 parameters as the initial input.

Briefly, our interest is in a purely electronic structure description of the PES, which necessitates exclusion of thermal and zero-point energy contributions. The latter are included via classical molecular dynamics simulations and quantum Monte Carlo (MC) simulations. Therefore, the semiempirical energies of the molecules, which are traditionally expressed in terms of heats of formation, were interrelated by means of the *difference* in electronic energy between respective compounds at the target level. More specifically, carbon dioxide and neutral nicotinamide were used as reference species, and their target

semiempirical energies were arbitrarily set to the actual heats of formation reported in the literature. This may be viewed as adding a constant number to their respective electronic energies. The other model molecules are energetically related to the reference molecules solely by means of the difference in electronic energy (including conformational transitions, protonation/deprotonation or introduction/abstraction of a hydride). The rationale for using the experimental heats of formation for these two molecules is to generate absolute energies that are close to the initial AM1 absolute energies. Such an approach limits the parameter search space to values near those of the canonical AM1 Hamiltonian, which performs reasonably well for many properties. Subsequently, the semiempirical energies of their chemically related compounds, formed by introducing a proton (i.e., protonated species) or a hydride, were determined by satisfying the following equality requirements:

$$E^{\text{SRP}}(\text{R}) - E^{\text{SRP}}(\text{RH}^+)$$
$$= E_{el}^{\text{G4MP2}}(\text{R}) - E_{el}^{\text{G4MP2}}(\text{RH}^+) - \Delta H_f^{\text{exp}}(\text{H}^+) \quad (2a)$$

$$E^{\text{SRP}}(\text{R}) - E^{\text{SRP}}(\text{RH}^-)$$
$$= E_{el}^{\text{G4MP2}}(\text{R}) + E_{el}^{\text{G4MP2}}(\text{H}^-) - E_{el}^{\text{G4MP2}}(\text{RH}^-)$$
$$- \Delta H_f^{\text{exp}}(\text{H}^-) \quad (2b)$$

Here $E^{\text{SRP}}(\text{R})$, $E^{\text{SRP}}(\text{RH}^+)$, and $E^{\text{SRP}}(\text{RH}^-)$ stand for the respective target semiempirical energies of the reference molecule, R, and its protonated counterpart, RH$^+$, or the reduced compound, RH$^-$; E_{el}^{G4MP2} is the electronic energy of either of the aforementioned molecules calculated at the G4MP2 level of theory; and $\Delta H_f^{\text{exp}}(\text{H}^+)$ and $\Delta H_f^{\text{exp}}(\text{H}^-)$ are the experimental enthalpies of formation of proton (365.7 kcal/mol)[54] and hydride (34.7 kcal/mol).[55] The specific goal of these expressions is to reproduce the proton or hydride affinity from the *ab initio* calculations, rather than reproducing the *absolute* heats of formations. A thorough derivation and explanation of eqs 2a and 2b is provided elsewhere[53] (see the Supporting Information therein).

2.2. QM/MM Simulations of *Pse*FDH. The crystal structure of *Pse*FDH dimer with the azide inhibitor and the cofactor NAD$^+$ (PDB ID code 2nad),[12] was used to construct the initial configuration for the present study. The X-ray crystal structure contains 391 amino acid residues in monomer A and 383 amino acid residues in monomer B, 830 crystallographic waters, the azide and NAD$^+$ ligands.[12] The azide and NAD$^+$ ligands were replaced by CO$_2$ and NADH, respectively, in each monomer, for the simulation. The missing crystallographic residues 392−393 and 384−393 were added to monomer A and monomer B, respectively, using Discovery Studio 3.0 (Accelrys Inc.), prior to commencing simulations.

The protonation states for all ionizable residues were set corresponding to pH 7.[6] The hydrogen bonding patterns of the ionizable residues with the surrounding environment were visually inspected to verify that the protonation states are reasonable. The coordinates of hydrogen atoms of the protein, water, and coenzyme were determined using the HBUILD facility in the program CHARMM.[56,57] The possible protonation states of histidine residues (proton on Nε, proton on Nδ or doubly protonated form) were determined by examination of the hydrogen bonding interactions. Peripheral/surface His residues were generally assumed to be positively charged. The

resulting negatively charged enzyme (-14) has dimensions of ca. $56 \times 66 \times 98$ Å^3. To this system we added 14 sodium ions in random positions outside the protein to obtain a net-neutral system.[58] Subsequently, the protein, ligands, crystal waters, and counterions were embedded in a water box as detailed below.

Hybrid QM(SRP)/MM Potential Energy Surface. The hydride transfer reaction in FDH was described using a hybrid QM/MM PES.

$$\hat{H} = \hat{H}_{QM} + \hat{H}_{MM} + \hat{H}_{QM/MM} \qquad (3)$$

The system was partitioned into a QM region consisting of 33 atoms and a MM region containing the rest of the system. The QM subsystem includes 3 atoms from the CO$_2$ substrate and 29 atoms from the NADH coenzyme (the dihydronicotinamide and ribose moiety). Additionally, one hydrogen link atom was introduced along the covalent bonds crossing the boundary between the QM and MM regions, to satisfy the valence requirements of the QM fragments. A schematic representation is depicted in Figure 1, where the quantum link atom is encircled.
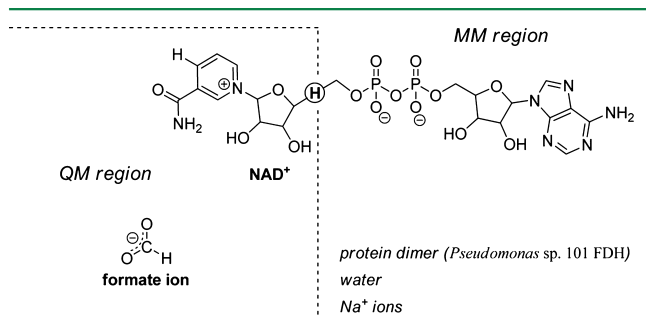
Figure 1. QM/MM partitioning scheme. The dashed line divides the QM and MM regions, and the quantum hydrogen link atom is circled.

The QM region was treated by the AM1-SRP Hamiltonian described above. The all-atom CHARMM22 force field[59] with grid-based energy correction maps (CMAP)[60] for peptide dihedral angles was employed to treat the entire protein, the substrate, and the ions, while the CHARMM27 force field[59,61,62] was used for the coenzyme. The water molecules were represented by the three-point charge TIP3P model.[63] QM/MM interactions were treated by electrostatic embedding wherein the MM partial atomic charges are included in the one-electron Hamiltonian.

Free-Energy Simulations - General Approach.[35] We follow a two-step procedure in which we first carry out Newtonian MD simulations to determine the classical mechanical potential of mean force (PMF) along the reaction coordinate for the hydride transfer reaction between formate and NAD$^+$ in the fully solvated enzyme. Subsequently, atoms directly involved in the hydride transfer are quantized via centroid path-integral simulations. To this end, configurations sampled in the classical MD simulations are used as a configuration basin for the quantum simulations. This double (quantum and classical) averaging scheme is formally exact[35,64−66] and yields the QM-PMF as a function of the centroid reaction path.[67,68] In PI-FEP/UM, the ratio of the quantum partition functions for different isotopes, which yields the kinetic isotope effects (KIEs), is obtained by free-energy perturbation from a light isotope mass into a heavier one within the same centroid path-integral simulation,[35] avoiding the difference between two free-

energy barriers with greater fluctuations than the difference itself for the two isotopic reactions.[33,35]

MD Simulations. MD simulations were conducted under periodic boundary conditions (PBC), with Ewald summation for electrostatic interactions.[69] The solute was soaked in a pre-equilibrated $92 \times 92 \times 92$ Å^3 cubic box of 26,784 water molecules, with its longest axis lying along the space diagonal of the box to ensure that all protein atoms are at least 10 Å away from the edges of the box. The final model contained 79,620 atoms. For van der Waals and electrostatic interactions, a 13.0 Å group-based cutoff was used. The Ewald method was employed for reciprocal space summations between MM sites as well as for the QM/MM interactions using a $90 \times 90 \times 90$ FFT grid.[69] The κ value was set to 0.340 Å^{-1}.

All water molecules were relaxed using the adopted-basis set Newton−Raphson (ABNR) minimization method (30 steps), while the crystal water oxygens were harmonically restrained to their original positions. This was followed by a 100 ps MD equilibration of the water molecules, which were thereafter minimized again (30 steps ABNR). All atoms were subsequently subjected to a stepwise minimization, to remove close contacts in the initial protein−ligand-solvent system.

The isothermal−isobaric ensemble (NPT) was employed at 1 atm and 310 K using the extended system pressure/temperature (CPT) algorithm of Andersen[70] with an effective mass of 500 amu and Hoover thermostat[71] with an effective mass of 1,000 kcal/mol·ps^2. The SHAKE algorithm[72] was applied to constrain all MM bonds involving hydrogen atoms. The system was gradually heated from 48 to 310 K during five sessions of 5 ps for a total of 25 ps and thereafter equilibrated at the target temperature (310 K) over the course of 1 ns at the MM level of theory, with further 200 ps of equilibration using the QM(AM1-SRP)/MM potential.

Potential of Mean Force. The classical-mechanical potential of mean force (CM-PMF)[73] was determined using the umbrella sampling technique, in order to sample the high-energy regions of the PES.[74] The reaction coordinate (ζ) was defined as a collective reaction coordinate.[75] This collective coordinate is composed of three reaction coordinates. The first is the antisymmetric stretch coordinate, which is defined geometrically as the difference between the lengths of the breaking (H4N − C$_{HCOO^-}$) and forming (C4N$_{NAD^+}$ − H4N) bonds.

$$\zeta_{asym} = R(C - H4N) - R(C4N - H4N) \qquad (4)$$

The second reaction coordinate considered is the donor−acceptor distance (DAD)

$$\zeta_{DAD} = R(C - C4N) \qquad (5)$$

Finally, the third reaction coordinate describes the difference between the hybridization states (defining the extent of the p vs s atomic orbital contributions to the hybrid orbital), χ,[76] of the hydride donor (C) and hydride acceptor (C4N) carbon atoms

$$\zeta_{rehyb} = \chi(C4N) - \chi(C) \qquad (6)$$

As this quantity expresses the relative hybridization, we shall refer to the definition in eq 6 as the rehybridization coordinate.

The hybridization state can be linearly correlated with L, the distance from the central carbon atom to the line or plane, determined by the positions of its substituents (excluding the position of the transferring hydride), in the form

$$\chi(C4N) = 2 + 3L_{acceptor} \qquad (7)$$

for the acceptor C4N carbon, and in the form

$$\chi(C) = 1 + 2L_{donor} \qquad (8)$$

for the donor C carbon.

Taking advantage of this definition, we note that substitution of eq 7 and eq 8 into eq 6 yields

$$\zeta'_{rehyb} = 3L_{acceptor} - 2L_{donor} + 1 \qquad (9)$$

Practically, we used the form

$$\zeta_{rehyb} = 3L_{acceptor} - 2L_{donor} \qquad (10)$$

for all calculations mentioned in this study involving the rehybridization coordinate. More specifically, in the RS of the FDH catalyzed reaction, both the C4N (hydride acceptor) and C (hydride donor) carbons adopt approximate sp^2 hybridizations, respectively, which correspond to $\chi(C4N) = 2$, $L_{acceptor} = 0$ Å and $\chi(C) = 2$, $L_{donor} = 1/2$ Å. Accordingly, the lower boundary of ζ_{rehyb} will be given a theoretical value of -1 Å; whereas, the PS is inevitably characterized by tetrahedral symmetry of C4N and linear geometry of C, i.e. $\chi(C4N) = 3$, $L_{acceptor} = 1/3$ Å and $\chi(C) = 1$, $L_{donor} = 0$ Å, resulting in an upper limit value of 1 Å.

The PMF is described as a function of these three reaction coordinates. The collective reaction coordinate is defined as the minimum free energy path in the multidimensional reaction coordinate space. Practically, this path is obtained using the zero-temperature string method, which is adapted to the numerical data representation of the free energy surface.[75] A total of 14 discrete regions along the reaction coordinate ("windows") were defined with spacing of ca. 0.25 Å. Each simulation was performed with the addition of a biasing potential to the antisymmetric stretch coordinate (roughly the negative of the computed PMF) and a harmonic restraint centered in each window. The harmonic force constants, k, ranged between 5.0−80.0 kcal·mol^{-1}·Å^{-2} [$E_{harm} = k(\zeta - \zeta_{ref})^2$]. Each window was equilibrated for 200 ps, followed by a 200 ps production simulation that collected the probability densities of configurations (ρ) along the reaction coordinates (ζ_i), and sorted them into bins of width 0.01−0.04 Å. The coordinates were saved every 0.1 ps, and the velocities and positions of the last configuration generated in each window were used to initiate the next window. The PMF curve was obtained using a multidimensional version of the Weighted Histogram Analysis Method (WHAM).[75,77] To ensure convergence of the PMF, the simulations were run until the difference between sequential PMF profiles was less than ±1 kcal/mol.

The QM-PMF was obtained using a double averaging procedure by centroid path-integral simulations on configurations saved during the umbrella sampling.[35,65,78] In essence, the centroid path-integral simulations yield the free energy difference between the classical mechanical and the quantum mechanical PMFs.[35,65] For each isotope, a quantized correction curve was fit to the PI simulation data using an inverted Eckart function. The curve fitting was done using the Levenberg−Marquardt algorithm, and the inverted Eckart potential was added to the CM-PMF to obtain the QM-PMF.

Kinetic Isotope Effects. For the primary KIE, the hydrogen originally covalently bonded to the formate ion's carbon in the reactant state of the FDH-catalyzed reaction (the donated hydride, labeled H4N in Chart 1) is substituted with deuterium (k_H^H/k_D^H) and tritium (k_H^H/k_T^H). For the secondary KIE, the hydrogen located at the 4-position of the pyridine ring in NAD$^+$

(labeled H42N in Chart 1) is substituted with deuterium (k_H^H/k_D^H) and tritium (k_H^H/k_T^H). An integrated centroid path integral and free-energy perturbation-umbrella sampling (PI-FEP/UM) method was used to compute KIEs.[35] The method is based on quantum transition state theory and uses the bisection or staging sampling algorithms coupled with a mass-perturbation scheme to compute KIEs directly.[35]

Specifically, to evaluate the KIEs, the centroid path-integral simulations were carried out for the light isotopic reaction, and the ratio of the partition functions between two isotopic reactions was determined by free-energy perturbation theory from the light mass into a heavier one.[35] In the present study, we quantized the donor (C_{HCOO^-}) and acceptor ($C4N_{NAD^+}$) carbons, in addition to the H4N hydrogen connected to the carboxylic acid donor carbon and the H42N hydrogen that is bonded to the acceptor carbon at the 4-position of the oxidized nicotinamide moiety (in the reactant state). Each quantized particle was represented by 32 beads. We used the staging sampling technique[78,79] in all centroid path-integral simulations. Ten free-particle configurations were sampled by Monte Carlo (MC) staging for each of ca. 5,000 classical configurations in the RS and TS, yielding a total of 100,000 path-integral sampling steps.

Vibrational Frequency Calculations. To estimate the effect of the enzyme environment on the TS in FDH, we calculated the antisymmetric stretch frequency for an azide ion in the gas phase, in aqueous solution, and in FDH. We computed the one-dimensional QM/MM potential, $V(\zeta_{asym})$, as a function of the antisymmetric normal mode coordinate for azide. Specifically, we employed a thermal density matrix approach which was solved for the antisymmetric stretch potential to yield the normal mode eigenvalues.[38] The stretch frequency in water and FDH was computed as an average of 1,000 structures taken from a 50 ps MD simulation. Prior to this the structures were equilibrated for 1.5−2.0 ns. The azide was treated by the PM3-AZI parametrization, used in the study of carbonic anhydrase.[80]

3. RESULTS AND DISCUSSION

3.1. Gas-Phase QM Calculations. *Model Reactions.* In Table 1, the calculated energies, enthalpies, and free energies at room temperature are given for the model reactions involving N-methyl substituted nicotinamides. The results are reported separately for each of the two thermodynamic pathways described in the methods section (eq 1).

Table 1. Energetics (kcal/mol) Calculated for FDH Model Reactions in the Gas Phase^c

method	cisoid → cisoid^a			transoid → transoid^b		
	ΔE_{el}	ΔH_r	ΔG_r	ΔE_{el}	ΔH_r	ΔG_r
AM1	−132.0	−130.8	−129.4	−131.6	−130.5	−127.6
AM1-SRP	−126.9	−127.1	−123.1	−126.2	−125.3	−123.6
M06/6-31+G(d,p)	−124.1	−123.1	−121.7	−123.7	−122.9	−121.9
G4MP2	−124.6	−123.9	−122.1	−125.3	−124.5	−122.7
CBS-QB3	−123.6	−122.8	−121.1	−124.2	−123.4	−121.7

^{a}HCOO$^-$ + *cis*-Me-Hnic$^+$ ⇌ CO$_2$ + *cis*-Me-H$_2$nic. ^{b}HCOO$^-$ + *trans*-Me-Hnic$^+$ ⇌ CO$_2$ + *trans*-Me-H$_2$nic. $^c\Delta E_{el}$ is the change in electronic energy; ΔH_r and ΔG_r are the respective enthalpy and free energy changes at 298.15 K and 1 atm (including zero-point contributions).

All methods predict a highly exothermic (and exergonic) reaction for the model reaction. There is no significant difference between the absolute magnitude of the *cisoid* → *cisoid* and *transoid* → *transoid* reactions. The results obtained with CBS-QB3 and G4MP2 are very similar. The M06 functional yields results similar to G4MP2 and is closest to the *ab initio* data among a range of DFT methods tested (results not shown). The standard semiempirical AM1 Hamiltonian gives a reaction that is too exothermic.

To obtain an efficient, yet accurate semiempirical parametrization, the AM1 parameters were calibrated against various electronic and energetic properties that were calculated with the high-level G4MP2 composite method[46,47] as well as the M06 method with the 6-31+G(d,p) basis set.[43] The target data set included heats of formation, relative energies, geometries, dipole moments, Mulliken charges, and vibrational frequencies of the individual species.

The relative energies obtained using AM1-SRP show good agreement with CBS-QB3 and in particular G4MP2 as shown in Table 1. Table 2 provides further insight into the

Table 2. Target Semiempirical Absolute Energies and the Actual Energies Obtained with the Optimized AM1-SRP Model (kcal/mol)

group	compound	target	optimized
one-carbon molecules	CO_2	−94.1[a]	−81.9
	$HCOO^-$	−128.6	−113.4
methyl nicotinamides	*cis*-Me-H_2nic	−11.6[b]	−20.1
	cis-Me-Hnic$^+$	147.6	142.5
	trans-Me-H_2nic	−10.3	−17.7
	trans-Me-Hnic$^+$	149.5	144.3
unsubstituted nicotinamides	*cis*-H_2nic	−33.7	−25.5
	cis-Hnic$^+$	131.8	140.2
	trans-H_2nic	−32.4	−23.0
	trans-Hnic$^+$	133.4	141.7
neutral nicotinamides	*cis*-nic	−6.1	−12.7
	trans-nic	−6.9[c]	−13.0

[a]Internal reference, the experimental enthalpy of formation of carbon dioxide in the gaseous state at 298 K.[83] [b]Internal reference, calculated as the enthalpy of formation in the gaseous state at 298 K at the G4MP2 level. [c]Internal reference, the experimental enthalpy of formation of nicotinamide in the gaseous state at 298 K.[84]

performance of the AM1-SRP model. The absolute energies of the individual molecules obtained with AM1-SRP are in fair agreement with the target values. We stress that the goal in the SRP development process is to obtain accurate relative energies and various properties, while preserving reasonable absolute energies.

Table 3 compares the root-mean-square deviations (rmsd) from the target data (G4MP2) for various properties calculated for the optimized geometries at the AM1 and AM1-SRP levels. The main achievement of the SRP model is to correct the relative energy computed at the AM1 level, which is too exothermic prior to reparametrization. Additionally, the vibrational wavenumbers and dipole moments are improved, without significantly reducing the accuracy in properties such as geometry and charge distribution, which are treated reasonably well at the AM1 level.

Reaction, Transition, and Product Complexes. The diagram in Figure 2 compares the relative energies of the reactant, transition, and product states (RS, TS, and PS), for

Table 3. RMSD Errors for Properties Calculated at Optimized Geometries Using AM1 and AM1-SRP with Respect to Target Values (G4MP2)

properties	AM1	AM1-SRP
absolute energies[a] (kcal/mol)	10.1	9.7
relative energies[b] (kcal/mol)	6.9	1.8
bond lengths[a] (Å)	0.02	0.02
bond angles[a] (deg)	1.6	1.5
vibrational wavenumbers[c] (cm^{-1})	135	124
Mulliken atomic charges[a] (e)	0.11	0.16
dipole moments[a] (D)	0.36	0.14

[a]The statistics refer to all 12 individual species. [b]The statistics refer to the reactions described in Table 1. [c]The statistics refer to wavenumbers larger than 2500 cm^{-1} for all 12 individual species.
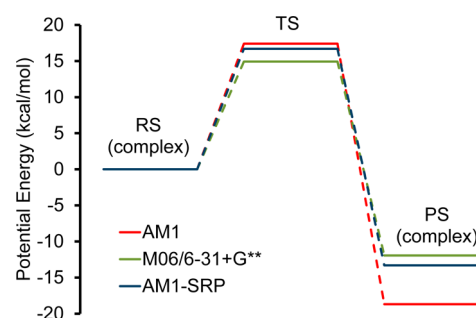

Figure 2. The relative energies (kcal/mol) of the reactant, transition, and product states associated with the reaction $HCOO^-$ + *trans*-Me-Hnic$^+$ → CO_2 + *trans*-Me-H_2nic. RS (complex) and PS (complex) refer to the reactant and product state bimolecular complexes.

the reaction $HCOO^-$ + *trans*-Me-Hnic$^+$ → CO_2 + *trans*-Me-H_2nic in a continuum water solvent, using AM1, AM1-SRP, and M06/6-31+G(d,p).

Focusing on the bimolecular complexes, we define the energy barrier, $\Delta E^{\ddagger}$, as the energy gap between the TS and RS complexes, and the reaction energy ΔE_r as the difference between the PS and RS complexes. For the standard AM1 method, there is an energy barrier of 17.4 kcal/mol and an exothermic reaction of −18.7 kcal/mol. The DFT method, M06, predicts a barrier of 14.9 kcal/mol and an exothermic reaction of −12.8 kcal/mol. For the AM1-SRP method, there is an energy barrier of 16.7 kcal/mol and an exothermic reaction of −13.3 kcal/mol. The imaginary vibrational frequencies at the TS are −1129.3 cm^{-1}, −1488.2 cm^{-1}, and −1455.7 cm^{-1} using M06, AM1, and AM-SRP, respectively. The discrepancy between the DFT and semiempirical methods may be ascribed to a difference in orientation of the carboxylate moiety relative to the nicotinamide ring using the three methods (Tables S27, S30, and S33). A weak hydrogen bond is formed at the TS between the carboxylate and amide groups with M06, resulting in a lower imaginary frequency. This slightly reduced hydrogen bond capacity with AM1-SRP is not expected to be of importance in FDH simulations, where the reactive fragments are held in place by strong QM/MM interactions with the enzyme. In conclusion, the AM1-SRP method corrects the main deficiency in the canonical AM1 for the FDH reaction.

3.2. Enzyme Simulations. *Classical Potential of Mean Force.* Figure 3 shows the one-dimensional classical mechanical PMF (CM-PMF) for the FDH-catalyzed hydride transfer reaction obtained from free energy MD simulations, using the AM1 and AM1-SRP QM/MM Hamiltonians. Specifically, when
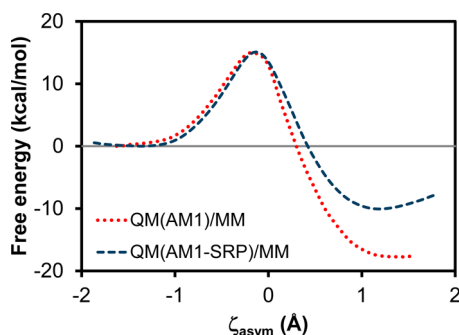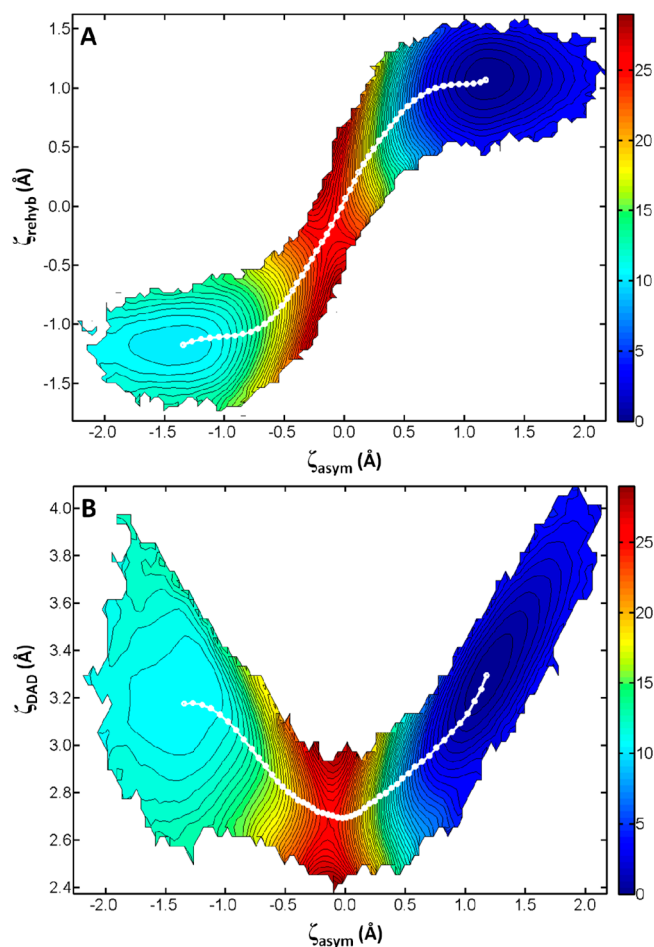
Figure 3. Computed classical potentials of mean force (kcal/mol) for the hydride transfer reaction catalyzed by *Pse*FDH at 310 K, obtained with two QM/MM schemes distinguished by the semiempirical treatment of the QM region: AM1/MM (red) and AM1-SRP/MM (blue). The reaction coordinate is defined as the difference between the distances of the transferring hydride and the donor and acceptor carbon atoms.

the QM(AM1-SRP)/MM Hamiltonian is employed, the free energy barrier predicted by the corresponding PMF ($\Delta G^{\ddagger}$ = 15.1 kcal/mol) is almost identical to that obtained when the atoms in the QM region are treated with the standard AM1 potential. In this regard, it is noteworthy that single-point MP2(6-31G**)/MM calculations performed by Moliner and co-workers[10] (based on preoptimized HF/MM geometries of the RS and TS) afforded a similar energy of activation (12.4 kcal/mol) as obtained by them at the AM1 level. We also emphasize that the aforementioned classical free energy barrier does not account for nuclear quantum effects, such as zero-point energy and tunneling. Using QM(AM1-SRP)/MM we obtain a relatively early TS, located at ca. ζ_{asym} = −0.15 Å. On the other hand, the differences in the free energies of reaction are notable, with QM(AM1-SRP)/MM yielding ΔG_r = −10.1 kcal/mol. This corresponds to a reduced exergonicity by ca. 8 kcal/mol relative to that calculated using a QM(AM1)/MM PES.

To obtain further insight into the change in hybridization and DAD during the catalytic reaction, we present a pair of two-dimensional free energy surfaces in Figure 4. In Figure 4A we present the free energy as a function of the antisymmetric stretch coordinate and the rehybridization coordinate. It is clear from this figure that progress along the chemical coordinate (i.e., antisymmetric stretch) and environmental coordinate (i.e., rehybridization) are not fully synchronized. Indeed, the rehybridization lags behind the antisymmetric stretch coordinate in the reactant and products wells. However, near the TS the hydride progress coordinate and the rehybridization coordinate are synchronized. A similar picture has been observed for DHFR previously.[75,76] The correlation between rehybridization and reaction progress is also illustrated in Figure 5 where one can see the change in hybridization states at the cofactor C4N and substrate C carbons as a function of the antisymmetric stretch coordinate. In Figure 5 we observe a smooth progress from sp^2 hybridization in the RS to sp^3 and sp hybridization for C4N and C, respectively, in the PS. The average hybridization state remains constant at ca. 2, with a slight peak around the TS. This peak is due to a faster rehybridization at the C4N carbon than at the C position. In Figure 4B we present the free energy as a function of the antisymmetric stretch coordinate and the DAD coordinate. The expected shortening of the DAD as the reaction approaches the

Figure 4. Computed classical two-dimensional potentials of mean force (kcal/mol) for the hydride transfer reaction catalyzed by *Pse*FDH at 310 K using QM(AM1-SRP)/MM. (A) Free energy as a function of the antisymmetric stretch and rehybridization coordinates. (B) Free energy as a function of the antisymmetric stretch and donor−acceptor distance coordinates. The contour lines in each surface are spaced by 0.5 kcal/mol. The minimum free energy path (white) was obtained using the zero-temperature string method with 50 images.[85]
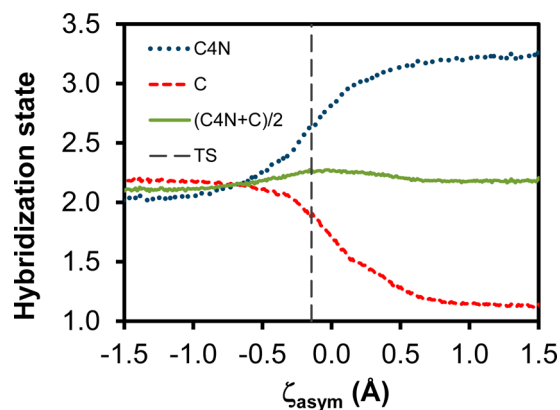

Figure 5. The variation of the hybridization states of the donor (C4N) and acceptor (C) carbons and their average value along the antisymmetric stretch coordinate, ζ_{asym}. The vertical dashed line corresponds to the location of the transition state.

TS is observed, while the RS and PS wells are symmetrically positioned around the TS. Additionally, the variation of the free

energy at the TS with the DAD is rather small, suggesting a range of classically allowed DADs at the dividing surface.

Quantum Potential of Mean Force. The QM-PMF is obtained from centroid Feynman path-integral calculations,[35,64,66] in which the centroid positions of the discrete paths of quantized particles are used to specify the reaction coordinate.[35,67,68] The quantum free energy profiles displayed in Figure 6 describe the hydride transfer reaction with the SRP
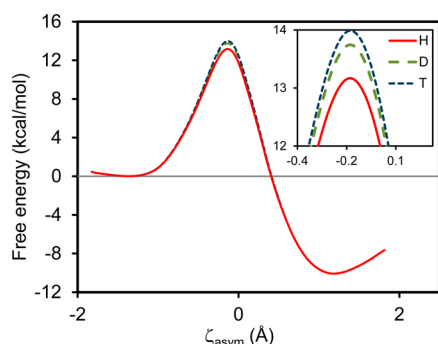
Figure 6. Computed quantum potentials of mean force (kcal/mol) for the hydride transfer reaction catalyzed by *Pse*FDH at 310 K for different isotopes: hydride, deuteride, and triteride. The reaction coordinate is defined as the difference between the distances of the centroids of the transferring hydride and the donor and acceptor carbon atoms.

QM/MM Hamiltonian. Using QM(AM1-SRP)/MM, inclusion of NQE in the simulations[35] lowers the computed free energies of activation for the hydride, deuteride, and tritium transfer by 1.9, 1.4, and 1.1 kcal/mol, respectively, relative to the classical free energy barrier (see Table 4). The resulting quantum free

Table 4. Free Energies of Reaction, ΔG_r, and Activation, $\Delta G^{\ddagger}$ (kcal/mol), Calculated from Nuclear Classical Mechanical (NCM) and Quantum Mechanical (NQM) Potentials of Mean Force for the Hydride Transfer Reaction in *Pse*FDH Based on the QM(AM1-SRP)/MM Hamiltonian[a]

| | QM(AM1-SRP)/MM | | | | |
| | | NQM | | | |
	NCM	H	D	T	Exp[2,8]
ΔG_r	−10.1	−10.1	−10.1	−10.1	--
$\Delta G^{\ddagger}$	15.1	13.2	13.7	14.0	16.6

[a]The QM data are shown for the hydride (H), deuteride (D), and triteride (T) isotopomers.

energies of reaction and activation for the hydride transfer are −10.1 and 13.2 kcal/mol. The difference in reaction free energy between the different isotopomers is small (<0.1 kcal/mol), as expected based on the small equilibrium isotope effect.[27] While our prediction for the free energy of activation approaches that measured experimentally (16.6 kcal/mol),[2,6] our result corresponds exclusively to the hydride transfer step rather than reflecting a phenomenological complex multistep rate constant. As pointed out by Moliner and co-workers,[10] the intrinsic rate of the formate oxidation reaction computed herein differs from the experimentally measured rate constant. Indeed, k_{cat} may be masked by other nonchemical kinetic steps which contribute individually to the overall rate constant. The free-energy results suggest that the present QM(AM1-SRP)/MM

and path integral methods can provide an adequate description of the hydride transfer reaction in FDH.

Kinetic Isotope Effects. The computed intrinsic primary H/D, H/T, and D/T KIEs for the hydride transfer reaction in FDH at 310 K are 3.43 ± 0.41, 5.20 ± 0.90, and 1.71 ± 0.08 with QM(AM1-SRP)/MM, respectively. These values, as shown in Table 5, are in good agreement with the experimental

Table 5. Primary and Secondary KIE Values for the Hydride Transfer Reaction in FDH at 310 K

| | 1° KIE | | 2° KIE | |
	calcd	exp[8]	calcd	exp[28]
H/D	3.43 ± 0.41	3.41 ± 0.30	1.12 ± 0.12	1.23 ± 0.03
H/T	5.20 ± 0.90	5.88 ± 0.75	1.15 ± 0.18	--
D/T	1.71 ± 0.08	1.70 ± 0.06	1.02 ± 0.04	--

intrinsic KIEs measured by Kohen and co-workers for the related *Cbo*FDH (H/D = 3.41 ± 0.30, H/T = 5.88 ± 0.75, and D/T = 1.70 ± 0.06),[8] providing additional evidence for the accuracy of our computational treatments. These primary H/D values are somewhat higher than the primary H/D KIEs measured by Cleland and co-workers[28] (2.27 ± 0.21). The small deflation of those observed KIEs is attributed to the difference between the intrinsic KIE and the experimentally observed value by Cleland and co-workers, which are masked by some kinetic complexity.

The computed secondary H/D, H/T, and D/T KIEs for the hydride transfer in FDH at 310 K are 1.12 ± 0.12, 1.15 ± 0.18, and 1.02 ± 0.04 with QM(AM1-SRP)/MM, respectively. The H/D value is in reasonable agreement with the experimental secondary H/D KIE measured by Cleland and co-workers[28] for yeast FDH (1.23 ± 0.03).

Azide Antisymmetric Stretch Vibration. The azide ion may be described by three valence bond (VB) structures:

$$\overset{=}{N} - \overset{+}{N} \equiv N \leftrightarrow \overset{-}{N} = \overset{+}{N} = \overset{-}{N} \leftrightarrow N \equiv \overset{+}{N} - \overset{=}{N}$$
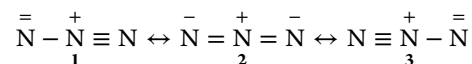
In the gas phase, the second VB structure contributes the most, while in a polar environment, structures 1 and 3 will contribute more.[80] The increased triple-bond character in structures 1 and 3 results in an observed blue shift in the antisymmetric vibrational frequency. In the gas phase we obtain a frequency of 2040 cm^{-1}, in fair agreement with the experimental value of 1987 cm^{-1}.[81] In aqueous solution we compute an ensemble average vibrational frequency of 2078 ± 9 cm^{-1}, comparable to 2049 cm^{-1} from experiment.[62] In FDH, the antisymmetric stretch frequency is similar to that in solution, with a value of 2065 cm^{-1} ± 11 cm^{-1}, comparable to 2043 cm^{-1} from experiment.[82] Importantly, both experiment and theory predict a slightly smaller blue shift in FDH than in water.

4. SUMMARY

In the current work we present benchmark calculations for model gas- and solution-phase reactions for the FDH catalyzed hydride transfer reaction. We employed G4MP2 and CBS-QB3 *ab initio* calculations as well as the M06 density functional method. Using these results as target data, we developed a specific reaction parameter (SRP) Hamiltonian by reparametrizing the semiempirical AM1 method. The SRP semiempirical Hamiltonian was consequently employed in hybrid quantum mechanics/molecular mechanics simulations of the FDH catalyzed reaction. Classical PMFs were computed using the

standard AM1 and the AM1-SRP methods. The PMF was expressed as a function of the antisymmetric stretch coordinate as well as an orbital rehybridization coordinate and a donor–acceptor distance coordinate. Based on these simulations we suggest that the reaction has an early TS and that hydride transfer and orbital rehybridization are not fully synchronized. To account for nuclear quantum effects, such as zero-point energy and tunneling, we employed centroid Feynman path-integral methods. Initially, quantum PMFs were obtained for hydride, deuteride, and triteride transfer reactions. Subsequently, kinetic isotope effects were computed using a mass-perturbation based path-integral approach. Finally, the antisymmetric vibrational frequency of an azide ion in FDH was computed and compared to that in the gas phase and water. The results presented herein are in good agreement with available experimental data, and we conclude that the resulting potential energy surface should be useful in simulations of the FDH catalyzed hydride transfer reaction.

■ ASSOCIATED CONTENT

Ⓢ Supporting Information

Multidimensional free energy surface; minimum free energy path; momentum distribution analysis; list of the optimized semiempirical parameters of AM1-SRP; coordinates of geometries calculated at the target levels and at the AM1-SRP level. This material is available free of charge via the Internet at http://pubs.acs.org.

■ AUTHOR INFORMATION

Corresponding Author
*E-mail: majort@biu.ac.il.

Notes
The authors declare no competing financial interest.

■ ACKNOWLEDGMENTS

■ REFERENCES

(1) Vinals, C.; Depiereux, E.; Feytmans, E. Prediction of structurally conserved regions of D-specific hydroxy acid dehydrogenases by multiple alignment with formate dehydrogenase. *Biochem. Biophys. Res. Commun.* **1993**, *192*, 182.

(2) Tishkov, V.; Popov, V. Catalytic mechanism and application of formate dehydrogenase. *Biochemistry (Moscow)* **2004**, *69*, 1252.

(3) Weckbecker, A.; Hummel, W. Improved synthesis of chiral alcohols with *Escherichia coli* cells co-expressing pyridine nucleotide transhydrogenase, NADP$^+$-dependent alcohol dehydrogenase and NAD$^+$-dependent formate dehydrogenase. *Biotechnol. Lett.* **2004**, *26*, 1739.

(4) Ernst, M.; Kaup, B.; Mueller, M.; Bringer-Meyer, S.; Sahm, H. Enantioselective reduction of carbonyl compounds by whole-cell biotransformation, combining a formate dehydrogenase and a (*R*)-specific alcohol dehydrogenase. *Appl. Microbiol. Biotechnol.* **2005**, *66*, 629.

(5) Bommarius, A. S.; Schwarm, M.; Stingl, K.; Kottenhahn, M.; Huthmacher, K.; Drauz, K. Synthesis and use of enantiomerically pure tert-leucine. *Tetrahedron: Asymmetry* **1995**, *6*, 2851.

(6) Popov, V. O.; Lamzin, V. S. NAD$^+$-dependent formate dehydrogenase. *Biochem. J.* **1994**, *301*, 625.

(7) Tishkov, V. I.; Popov, V. O. Protein engineering of formate dehydrogenase. *Biomol. Eng.* **2006**, *23*, 89.

(8) Bandaria, J. N.; Cheatum, C. M.; Kohen, A. Examination of enzymatic H-tunneling through kinetics and dynamics. *J. Am. Chem. Soc.* **2009**, *131*, 10151.

(9) Bandaria, J. N.; Dutta, S.; Hill, S. E.; Kohen, A.; Cheatum, C. M. Fast enzyme dynamics at the active site of formate dehydrogenase. *J. Am. Chem. Soc.* **2008**, *130*, 22.

(10) Castillo, R.; Oliva, M.; Marti, S.; Moliner, V. A theoretical study of the catalytic mechanism of formate dehydrogenase. *J. Phys. Chem. B* **2008**, *112*, 10012.

(11) Torres, R. A.; Schiøtt, B.; Bruice, T. C. Molecular dynamics simulations of ground and transition states for the hydride transfer from formate to NAD$^+$ in the active site of formate dehydrogenase. *J. Am. Chem. Soc.* **1999**, *121*, 8164.

(12) Lamzin, V. S.; Dauter, Z.; Popov, V. O.; Harutyunyan, E. H.; Wilson, K. S. High resolution structures of holo and apo formate dehydrogenase. *J. Mol. Biol.* **1994**, *236*, 759.

(13) Shabalin, I.; Filippova, E.; Polyakov, K.; Sadykhov, E.; Safonova, T.; Tikhonova, T.; Tishkov, V.; Popov, V. Structures of the apo and holo forms of formate dehydrogenase from the bacterium *Moraxella* sp. C-1: Towards understanding the mechanism of the closure of the interdomain cleft. *Acta Crystallogr., Sect. D: Biol. Crystallogr.* **2009**, *65*, 1315.

(14) Schirwitz, K.; Schmidt, A.; Lamzin, V. S. High-resolution structures of formate dehydrogenase from *Candida boidinii. Protein Sci.* **2007**, *16*, 1146.

(15) Tishkov, V. I.; Matorin, A. D.; Rojkova, A. M.; Fedorchuk, V. V.; Savitsky, P. A.; Dementieva, L. A.; Lamzin, V. S.; Mezentzev, A. V.; Popov, V. O. Site-directed mutagenesis of the formate dehydrogenase active centre: Role of the His332-Gln313 pair in enzyme catalysis. *FEBS Lett.* **1996**, *390*, 104.

(16) Galkin, A. G.; Kutsenko, A. S.; Bajulina, N. P.; Esipova, N. G.; Lamzin, V. S.; Mesentsev, A. V.; Shelukho, D. V.; Tikhonova, T. V.; Tishkov, V. I.; Ustinnikova, T. B.; Popov, V. O. Site-directed mutagenesis of the essential arginine of the formate dehydrogenase active centre. *Biochim. Biophys. Acta, Protein Struct. Mol. Enzymol.* **2002**, *1594*, 136.

(17) Li, H.; Goldstein, B. M. Carboxamide group conformation in the nicotinamide and thiazole-4-carboxamide rings: Implications for enzyme binding. *J. Med. Chem.* **1992**, *35*, 3560.

(18) Wu, Y. D.; Houk, K. N. Theoretical study of conformational features of NAD$^+$ and NADH analogs: Protonated nicotinamide and 1,4-dihydronicotinamide. *J. Org. Chem.* **1993**, *58*, 2043.

(19) Wu, Y. D.; Lai, D. K. W.; Houk, K. N. Transition structures of hydride transfer reactions of protonated pyridinium ion with 1,4-dihydropyridine and protonated nicotinamide with 1,4-dihydronicotinamide. *J. Am. Chem. Soc.* **1995**, *117*, 4100.

(20) Almarsson, O.; Sinha, A.; Gopinath, E.; Bruice, T. C. Mechanism of one-electron oxidation of NAD(P)H and function of NADPH bound to catalase. *J. Am. Chem. Soc.* **1993**, *115*, 7093.

(21) Almarsson, O.; Karaman, R.; Bruice, T. C. Kinetic importance of conformations of nicotinamide adenine dinucleotide in the reactions of dehydrogenase enzymes. *J. Am. Chem. Soc.* **1992**, *114*, 8702.

(22) Olson, L. P.; Bruice, T. C. Electron tunneling and ab initio calculations related to the one-electron oxidation of NAD(P)H bound to catalase. *Biochemistry* **1995**, *34*, 7335.

(23) Olson, L. P.; Luo, J.; Almarsson, Ö.; Bruice, T. C. Mechanism of aldehyde oxidation catalyzed by horse liver alcohol dehydrogenase. *Biochemistry* **1996**, *35*, 9782.

(24) Rotberg, N. S.; Cleland, W. Secondary nitrogen-15 isotope effects on the reactions catalyzed by alcohol and formate dehydrogenases. *Biochemistry* **1991**, *30*, 4068.

(25) Schiøtt, B.; Zheng, Y.-J.; Bruice, T. C. Theoretical investigation of the hydride transfer from formate to NAD$^+$ and the implications for the catalytic mechanism of formate dehydrogenase. *J. Am. Chem. Soc.* **1998**, *120*, 7192.

(26) Tapia, O.; Andrés, J.; Cardenas, R. Transition structure for the hydride transfer reaction from formate anion to cyclopropenyl cation: A simple theoretical model for the reaction catalyzed by formate dehydrogenase. *Chem. Phys. Lett.* **1992**, *189*, 395.

(27) Blanchard, J. S.; Cleland, W. Kinetic and chemical mechanisms of yeast formate dehydrogenase. *Biochemistry* **1980**, *19*, 3543.

(28) Hermes, J. D.; Morrical, S. W.; O'Leary, M. H.; Cleland, W. W. Variation of transition-state structure as a function of the nucleotide in reactions catalyzed by dehydrogenases. 2. Formate dehydrogenase. *Biochemistry* **1984**, *23*, 5479.

(29) Roca, M.; Oliva, M.; Castillo, R.; Moliner, V.; Tuñón, I. Do dynamic effects play a significant role in enzymatic catalysis? A theoretical analysis of formate dehydrogenase. *Chem.—Eur. J.* **2010**, *16*, 11399.

(30) Dewar, M. J. S.; Zoebisch, E. G.; Healy, E. F.; Stewart, J. J. P. AM1: A new general purpose quantum mechanical molecular model. *J. Am. Chem. Soc.* **1985**, *107*, 3902.

(31) Rossi, I.; Truhlar, D. G. Parametrization of NDDO wave-functions using genetic algorithms. An evolutionary approach to parameterizing potential energy surfaces and direct dynamics calculations for organic reactions. *Chem. Phys. Lett.* **1995**, *233*, 231.

(32) Major, D. T.; York, D. M.; Gao, J. L. Solvent polarization and kinetic isotope effects in nitroethane deprotonation and implications to the nitroalkane oxidase reaction. *J. Am. Chem. Soc.* **2005**, *127*, 16374.

(33) Gao, J. L.; Wong, K. Y.; Major, D. T. Combined QM/MM and path integral simulations of kinetic isotope effects in the proton transfer reaction between nitroethane and acetate ion in water. *J. Comput. Chem.* **2008**, *29*, 514.

(34) Warshel, A.; Levitt, M. Theoretical studies of enzymic reactions: Dielectric, electrostatic and steric stabilization of the carbonium ion in the reaction of lysozyme. *J. Mol. Biol.* **1976**, *103*, 227.

(35) Major, D. T.; Gao, J. L. An integrated path integral and free-energy perturbation-umbrella sampling method for computing kinetic isotope effects of chemical reactions in solution and in enzymes. *J. Chem. Theory Comput.* **2007**, *3*, 949.

(36) Major, D. T.; Gao, J. L. A combined quantum mechanical and molecular mechanical study of the reaction mechanism and alpha-amino acidity in alanine racemase. *J. Am. Chem. Soc.* **2006**, *128*, 16345.

(37) Major, D. T.; Heroux, A.; Orville, A. M.; Valley, M. P.; Fitzpatrick, P. F.; Gao, J. Differential quantum tunneling contributions in nitroalkane oxidase catalyzed and the uncatalyzed proton transfer reaction. *Proc. Natl. Acad. Sci. U.S.A.* **2009**, *106*, 20734.

(38) Engel, H.; Doron, D.; Kohen, A.; Major, D. T. Momentum distribution as a fingerprint of quantum delocalization in enzymatic reactions: Open-chain path-integral simulations of model systems and the hydride transfer in dihydrofolate reductase. *J. Chem. Theory Comput.* **2012**, *8*, 1223.

(39) Frisch, M. J.; Trucks, G. W.; Schlegel, H. B.; Scuseria, G. E.; Robb, M. A.; Cheeseman, J. R.; Scalmani, G.; Barone, V.; Mennucci, B.; Petersson, G. A.; Nakatsuji, H.; Caricato, M.; Li, X.; Hratchian, H. P.; Izmaylov, A. F.; Bloino, J.; Zheng, G.; Sonnenberg, J. L.; Hada, M.; Ehara, M.; Toyota, K.; Fukuda, R.; Hasegawa, J.; Ishida, M.; Nakajima, T.; Honda, Y.; Kitao, O.; Nakai, H.; Vreven, T.; Montgomery, J. A., Jr.; Peralta, J. E.; Ogliaro, F.; Bearpark, M.; Heyd, J. J.; Brothers, E.; Kudin, K. N.; Staroverov, V. N.; Kobayashi, R.; Normand, J.; Raghavachari, K.; Rendell, A.; Burant, J. C.; Iyengar, S. S.; Tomasi, J.; Cossi, M.; Rega, N.; Millam, N. J.; Klene, M.; Knox, J. E.; Cross, J. B.; Bakken, V.; Adamo, C.; Jaramillo, J.; Gomperts, R.; Stratmann, R. E.; Yazyev, O.; Austin, A. J.; Cammi, R.; Pomelli, C.; Ochterski, J. W.; Martin, R. L.; Morokuma, K.; Zakrzewski, V. G.; Voth, G. A.; Salvador, P.; Dannenberg, J. J.; Dapprich, S.; Daniels, A. D.; Farkas, Ö.; Foresman, J. B.; Ortiz, J. V.; Cioslowski, J.; Fox, D. J. *Gaussian 09, Revision B.01*; Gaussian, Inc.: Wallingford, CT, 2009.

(40) Becke, A. D. Density-functional thermochemistry. III. The role of exact exchange. *J. Chem. Phys.* **1993**, *98*, 5648.

(41) Lee, C.; Yang, W.; Parr, R. G. Development of the Colle-Salvetti correlation-energy formula into a functional of the electron density. *Phys. Rev. B: Condens. Matter Mater. Phys.* **1988**, *37*, 785.

(42) Stephens, P. J.; Devlin, F. J.; Chabalowski, C. F.; Frisch, M. J. *Ab initio* calculation of vibrational absorption and circular dichroism spectra using density functional force fields. *J. Phys. Chem.* **1994**, *98*, 11623.

(43) Zhao, Y.; Truhlar, D. The M06 suite of density functionals for main group thermochemistry, thermochemical kinetics, noncovalent interactions, excited states, and transition elements: Two new functionals and systematic testing of four M06-class functionals and 12 other functionals. *Theor. Chem. Acc.* **2008**, *120*, 215.

(44) Montgomery, J. J. A.; Frisch, M. J.; Ochterski, J. W.; Petersson, G. A. A complete basis set model chemistry. VI. Use of density functional geometries and frequencies. *J. Chem. Phys.* **1999**, *110*, 2822.

(45) Montgomery, J. J. A.; Frisch, M. J.; Ochterski, J. W.; Petersson, G. A. A complete basis set model chemistry. VII. Use of the minimum population localization method. *J. Chem. Phys.* **2000**, *112*, 6532.

(46) Curtiss, L. A.; Redfern, P. C.; Raghavachari, K. Gaussian-4 theory. *J. Chem. Phys.* **2007**, *126*, 084108.

(47) Curtiss, L. A.; Redfern, P. C.; Raghavachari, K. Gaussian-4 theory using reduced order perturbation theory. *J. Chem. Phys.* **2007**, *127*, 124105.

(48) McQuarrie, D. A. *Statistical Mechanics*; University Science Books: Sausalito, CA, 2000.

(49) Peng, C.; Schlegel, H. B. Combining synchronous transit and quasi-Newton methods to find transition states. *Isr. J. Chem.* **1994**, *33*, 449.

(50) Tomasi, J.; Mennucci, B.; Cammi, R. Quantum mechanical continuum solvation models. *Chem. Rev.* **2005**, *105*, 2999.

(51) Benach, J.; Atrian, S.; Gonzàlez-Duarte, R.; Ladenstein, R. The catalytic reaction and inhibition mechanism of *Drosophila* alcohol dehydrogenase: Observation of an enzyme-bound NAD-ketone adduct at 1.4 Å resolution by X-ray crystallography. *J. Mol. Biol.* **1999**, *289*, 335.

(52) Kavanagh, K. L.; Klimacek, M.; Nidetzky, B.; Wilson, D. K. Crystal structure of Pseudomonas fluorescens mannitol 2-dehydrogenase binary and ternary complexes. *J. Biol. Chem.* **2002**, *277*, 43433.

(53) Doron, D.; Major, D. T.; Kohen, A.; Thiel, W.; Wu, X. Hybrid quantum and classical simulations of the dihydrofolate reductase catalyzed hydride transfer reaction on an accurate semi-empirical potential energy surface. *J. Chem. Theory Comput.* **2011**, *7*, 3420.

(54) Lias, S.; Bartmess, J.; Liebman, J.; Holmes, J.; Levin, R.; Mallard, W. Gas-phase ion and neutral thermochemistry. *J. Phys. Chem. Ref. Data* **1988**, *17*, 1.

(55) Goebbert, D. J.; Wenthold, P. G. Gas-phase hydride affinities of neutral molecules. *Int. J. Mass Spectrom.* **2006**, *257*, 1.

(56) Brooks, B. R.; Bruccoleri, R. E.; Olafson, B. D.; States, D. J.; Swaminathan, S.; Karplus, M. CHARMM: A program for macro-molecular energy, minimization, and dynamics calculations. *J. Comput. Chem.* **1983**, *4*, 187.

(57) Brooks, B. R.; Brooks, C. L., III; MacKerell, A. D., Jr.; Nilsson, L.; Petrella, R. J.; Roux, B.; Won, Y.; Archontis, G.; Bartels, C.; Boresch, S.; Caflisch, A.; Caves, L.; Cui, Q.; Dinner, A. R.; Feig, M.; Fischer, S.; Gao, J.; Hodoscek, M.; Im, W.; Kuczera, K.; Lazaridis, T.; Ma, J.; Ovchinnikov, V.; Paci, E.; Pastor, R. W.; Post, C. B.; Pu, J. Z.; Schaefer, M.; Tidor, B.; Venable, R. M.; Woodcock, H. L.; Wu, X.; Yang, W.; York, D. M.; Karplus, M. CHARMM: The biomolecular simulation program. *J. Comput. Chem.* **2009**, *30*, 1545.

(58) Allen, M. P.; Tildesley, D. J. *Computer Simulation of Liquids*; Oxford University Press: Oxford, 1987; p 156.

(59) MacKerell, A. D., Jr.; Bashford, D.; Bellott, M.; Dunbrack, R. L., Jr.; Evanseck, J. D.; Field, M. J.; Fischer, S.; Gao, J.; Guo, H.; Ha, S.; Joseph-McCarthy, D.; Kuchnir, L.; Kuczera, K.; Lau, F. T. K.; Mattos, C.; Michnick, S.; Ngo, T.; Nguyen, D. T.; Prodhom, B.; Reiher, W. E.; Roux, B.; Schlenkrich, M.; Smith, J. C.; Stote, R.; Straub, J.; Watanabe, M.; Wiórkiewicz-Kuczera, J.; Yin, D.; Karplus, M. All-atom empirical potential for molecular modeling and dynamics studies of proteins. *J. Phys. Chem. B* **1998**, *102*, 3586.

(60) MacKerell, A. D., Jr.; Feig, M.; Brooks, C. L., III Extending the treatment of backbone energetics in protein force fields: Limitations of gas-phase quantum mechanics in reproducing protein conformational distributions in molecular dynamics simulations. *J. Comput. Chem.* **2004**, *25*, 1400.

(61) MacKerell, A. D., Jr.; Banavali, N. K. All-atom empirical force field for nucleic acids: II. Application to molecular dynamics

simulations of DNA and RNA in solution. *J. Comput. Chem.* **2000**, *21*, 105.

(62) Li, M.; Owrutsky, J.; Sarisky, M.; Culver, J. P.; Yodh, A.; Hochstrasser, R. M. Vibrational and rotational relaxation times of solvated molecular ions. *J. Chem. Phys.* **1993**, *98*, 5499.

(63) Jorgensen, W. L.; Chandrasekhar, J.; Madura, J. D.; Impey, R. W.; Klein, M. L. Comparison of simple potential functions for simulating liquid water. *J. Chem. Phys.* **1983**, *79*, 926.

(64) Major, D. T.; Garcia-Viloca, M.; Gao, J. L. Path integral simulations of proton transfer reactions in aqueous solution using combined QM/MM potentials. *J. Chem. Theory Comput.* **2006**, *2*, 236.

(65) Hwang, J. K.; Chu, Z. T.; Yadav, A.; Warshel, A. Simulations of quantum mechanical corrections for rate constants of hydride-transfer reactions in enzymes and solutions. *J. Phys. Chem.* **1991**, *95*, 8445.

(66) Major, D. T.; Gao, J. L. Implementation of the bisection sampling method in path integral simulations. *J. Mol. Graphics Modell.* **2005**, *24*, 121.

(67) Cao, J.; Voth, G. A. A unified framework for quantum activated rate processes. I. General theory. *J. Chem. Phys.* **1996**, *105*, 6856.

(68) Gillan, M. J. Quantum simulation of hydrogen in metals. *Phys. Rev. Lett.* **1987**, *58*, 563.

(69) Nam, K.; Gao, J.; York, D. M. An efficient linear-scaling Ewald method for long-range electrostatic interactions in combined QM/MM calculations. *J. Chem. Theory Comput.* **2005**, *1*, 2.

(70) Andersen, H. C. Molecular dynamics simulations at constant pressure and/or temperature. *J. Chem. Phys.* **1980**, *72*, 2384.

(71) Hoover, W. G. Canonical dynamics: Equilibrium phase-space distributions. *Phys. Rev. A: At., Mol., Opt. Phys.* **1985**, *31*, 1695.

(72) Ryckaert, J.-P.; Ciccotti, G.; Berendsen, H. J. C. Numerical integration of the cartesian equations of motion of a system with constraints: Molecular dynamics of *n*-alkanes. *J. Comput. Phys.* **1977**, *23*, 327.

(73) Pu, J.; Gao, J.; Truhlar, D. G. Multidimensional tunneling, recrossing, and the transmission coefficient for enzymatic reactions. *Chem. Rev.* **2006**, *106*, 3140.

(74) Torrie, G. M.; Valleau, J. P. Nonphysical sampling distributions in Monte Carlo free-energy estimation: Umbrella sampling. *J. Comput. Phys.* **1977**, *23*, 187.

(75) Doron, D.; Kohen, A.; Major, D. T. Collective reaction coordinate for hybrid quantum and molecular mechanics simulations: A case study of the hydride transfer in dihydrofolate reductase. *J. Chem. Theory Comput.* **2012**, *8*, 2484.

(76) Pu, J.; Ma, S.; Garcia-Viloca, M.; Gao, J.; Truhlar, D. G.; Kohen, A. Nonperfect synchronization of reaction center rehybridization in the transition state of the hydride transfer catalyzed by dihydrofolate reductase. *J. Am. Chem. Soc.* **2005**, *127*, 14879.

(77) Kumar, S.; Rosenberg, J. M.; Bouzida, D.; Swendsen, R. H.; Kollman, P. A. The weighted histogram analysis method for free-energy calculations on biomolecules. I. The method. *J. Comput. Chem.* **1992**, *13*, 1011.

(78) Sprik, M.; Klein, M. L.; Chandler, D. Staging - a sampling technique for the Monte-Carlo evaluation of path-integrals. *Phys. Rev. B: Condens. Matter Mater. Phys.* **1985**, *31*, 4234.

(79) Azuri, A.; Engel, H.; Doron, D.; Major, D. T. Path-integral calculations of nuclear quantum effects in model systems, small molecules, and enzymes via gradient based forward corrector algorithms. *J. Chem. Theory Comput.* **2011**, *7*, 1273.

(80) Garcia-Viloca, M.; Nam, K.; Alhambra, C.; Gao, J. Solvent and protein effects on the vibrational frequency shift and energy relaxation of the azide ligand in carbonic anhydrase. *J. Phys. Chem. B* **2004**, *108*, 13501.

(81) Polak, M.; Gruebele, M.; Saykally, R. J. Velocity modulation laser spectroscopy of negative ions: The ν_3 band of azide (N_3^-). *J. Am. Chem. Soc.* **1987**, *109*, 2884.

(82) Bandaria, J. N.; Dutta, S.; Nydegger, M. W.; Rock, W.; Kohen, A.; Cheatum, C. M. Characterizing the dynamics of functionally relevant complexes of formate dehydrogenase. *Proc. Natl. Acad. Sci. U.S.A.* **2010**, *107*, 17974.

(83) Chase, M. W., Jr. NIST-JANAF Thermochemical Tables, 4th ed.; *J. Phys. Chem. Ref. Data, Monograph 9*, **1998**.

(84) Ribeiro da Silva, M. D. M. C.; Gonçalves, J. M.; Ferreira, S. C. C.; da Silva, L. C. M.; Sottomayor, M. J.; Pilcher, G.; Acree, W. E., Jr.; Roy, L. E. Experimental thermochemical study of the enthalpies of formation and sublimation of isonicotinamide, picolinamide, nicotinamide, isonicotinamide *N*-oxide, and nicotinamide *N*-oxide. The dissociation enthalpies of the N-O bonds. *J. Chem. Thermodyn.* **2001**, *33*, 1263.

(85) E, W.; Ren, W.; Vanden-Eijnden, E. String method for the study of rare events. *Phys. Rev. B: Condens. Matter Mater. Phys.* **2002**, *66*, 052301.